Original article

Hormetic shifting of redox environment by pro-oxidative resveratrol protects cells against stress

CrossMark

Annabell Plauth [a], Anne Geikowski [a], Susanne Cichon [a], Sylvia J. Wowro [a], Linda Liedgens [a], Morten Rousseau [a], Christopher Weidner [a], Luise Fuhr [a], Magdalena Kliem [a], Gail Jenkins [b], Silvina Lotito [b], Linda J. Wainwright [b], Sascha Sauer [a,c,d,*]

[a] Otto Warburg Laboratory, Max Planck Institute for Molecular Genetics, 14195 Berlin, Germany
[b] Unilever R&D, Colworth Science Park, Sharnbrook, Bedfordshire MK44 1LQ, UK
[c] CU Systems Medicine, University of Würzburg, Josef-Schneider-Straße 2, Building D15, 97080 Würzburg, Germany
[d] Laboratory of Functional Genomics, Nutrigenomics and Systems Biology, BIMSB and BIH Genomics Platforms, Max-Delbrück-Center for Molecular Medicine, Robert-Rössle-Straße 10, 13125 Berlin, Germany

ABSTRACT

Resveratrol has gained tremendous interest owing to multiple reported health-beneficial effects. However, the underlying key mechanism of action of this natural product remained largely controversial. Here, we demonstrate that under physiologically relevant conditions major biological effects of resveratrol can be attributed to its generation of oxidation products such as reactive oxygen species (ROS). At low nontoxic concentrations (in general $< 50 \mu M$), treatment with resveratrol increased viability in a set of representative cell models, whereas application of quenchers of ROS completely truncated these beneficial effects. Notably, resveratrol treatment led to mild, Nrf2-specific gene expression reprogramming. For example, in primary epidermal keratinocytes derived from human skin this coordinated process resulted in a 1.3-fold increase of endogenously generated glutathione (GSH) and subsequently in a quantitative reduction of the cellular redox environment by 2.61 mV mmol GSH per g protein. After induction of oxidative stress by using 0.78% (v/v) ethanol, endogenous generation of ROS was consequently reduced by 24% in resveratrol pre-treated cells. In contrast to the common perception that resveratrol acts mainly as a chemical antioxidant or as a target protein-specific ligand, we propose that the cellular response to resveratrol treatment is essentially based on oxidative triggering. In physiological microenvironments this molecular training can lead to hormetic shifting of cellular defense towards a more reductive state to improve physiological resilience to oxidative stress.

© 2016 The Authors. Published by Elsevier Inc. This is an open access article under the CC BY-NC-ND license (http://creativecommons.org/licenses/by-nc-nd/4.0/).

1. Introduction

Polyphenols represent a large collection of natural products featuring health-beneficial effects [1]. Resveratrol (3,5,4′-trihydroxy-trans-stilbene, RSV), an antimicrobial phytoalexin originally found in white hellebore (*Veratrum grandiflorum O Loes*) and later in red grapes and other plants, is one of the most prominent polyphenols. Early studies indicated cancer chemo-preventive properties of RSV [2]. Over the last 15 years, numerous studies claimed additional benefits including cardio-protective and anti-aging effects [3]. Consequently, a number of products based on RSV have been developed for dietary and dermatological application [4,5]. Nevertheless, the efficiencies of RSV treatments and underlying mechanisms of action remained largely controversial. For example, RSV had been suggested to modulate estrogen receptor activity [6], or to act as a caloric mimetic by directly increasing the enzymatic activity of the histone deacetylase sirtuin 1 (SIRT1) [7]. Recently, it was shown that inhibition of phosphodiesterase 4 (PDE4) by RSV increased intracellular amounts of the hunger signalling molecule cAMP [8]. Notably, the reported interaction of RSV with these and further target proteins was in many cases low and unspecific. In general, most of these studies assumed a proportional dose-response relationship of compounds,

i.e. a conventional pharmacological (linear) threshold model [9].

However, in contrast to the standard pharmacological model, hundreds of studies reported (in many cases probably unconsciously) beneficial effects of RSV at "low" but detrimental outcomes at "high" doses. In general, this potentially counterintuitive bi-phasic property of RSV was widely ignored [10]. The large body of data would nevertheless hint to hormesis, a dose-response relationship that is characterized by low-dose stimulation and high-dose inhibition, consistent with the Arndt-Schulz law, Hueppe's rule and other terms describing a beneficial stimulation (of poisons) at low doses [11,12]. General acceptance of the hormesis concept for therapeutic application seems to remain minor, due to generally faint stimulatory effects and the lack of mechanistic explanation of hormetic phenomena.

Interestingly, polyphenols including RSV are considered as antioxidants mainly owing to chemical properties such as scavenging of free radicals or due to indirect effects in a given biological system. Depending on the chemical context RSV and other polyphenols can also become pro-oxidative [1], a fact that seems to be often ignored. Depending on the reaction conditions RSV can be (auto-) oxidized to generate semiquinones and the relatively stable 4′-phenoxyl radical; finally this oxidation process can lead to production of reactive oxygen species (ROS) [13,14]. Oxidative reactions of polyphenols are influenced by changing pH, particularly the presence of hydroxyl anions or organic bases [15,16]. Additionally, metal ions (e.g. iron II ions) facilitate oxidative reactions and generation of radicals via the Fenton reaction [17].

The here presented study aimed to explore new aspects and connect fragmented pieces of the chemical and resulting biological properties of RSV to contribute to a comprehensive understanding of the purported health-beneficial effects of RSV.

2. Material and methods

2.1. Materials

Chemical compounds were purchased from the following sources: Resveratrol (RSV; 3,5,4′-trihydroxy-trans-stilbene) and 4-hydroxy-2-nonenal (HNE) from Cayman Chemical (Biomol, Hamburg, Germany). Reduced glutathione (GSH) was purchased from Sigma Aldrich (Taufkirchen, Germany). The composition of Berlin tap water can be retrieved from: http://www.bwb.de.

2.2. Cell culture

Neonatal normal human epidermal keratinocyte cells (NHEK, CC-2503, Lonza, Basel, Swiss) were isolated from a black, newborn male. NHEK cells were maintained in keratinocyte growth medium (KGM) containing keratinocyte basal medium (KBM, CC-3101, Lonza) and KGM SingleQuot Kit Suppl. & Growth Factors (CC-4131, Lonza). Cells were treated with indicated compounds, vehicle (controls) were as follows: DMSO for RSV and EtOH for HNE (0.05% DMSO in case of 50 μM RSV; 0.78% ethanol in case of 25 μM HNE). GSH was dissolved in cell culture medium. Notably, hydrogen peroxide applied at low micromolar concentrations (comparable to HNE) did not produce any significant oxidative effects, probably due to efficient scavenging in the cellular context.

Neonatal normal human dermal fibroblast cells (NHDF, CC-209, Lonza) were isolated from a Caucasian, newborn male. NHDF cells were maintained in Dulbecco`s modified Eagle medium (# 31,966, Gibco, Life Technologies, Darmstadt, Germany) supplemented with 10% fetal bovine serum (FBS) Medium was renewed every two to three days and cells were split twice per week. Cells were treated at 60% confluence with 50 μM RSV or vehicle control.

Human HT-29 colon cells (ACC-299, DSMZ, Braunschweig, Germany) were cultured in Dulbecco's Modified Eagle Medium/ Nutrient Mixture F-12 (DMEM/F-12, # 11,330–057, Gibco, Life Technologies) supplemented with 5% FBS and 100 U/ml penicillin and 100 μg/ml streptomycin (all Biochrom, Berlin, Germany). *Human THP-1 monocyte cells* (ATCC, LGC Standards GmbH, Wesel, Germany) were cultivated in RPMI 1640 (Biochrom) supplemented with 10% FBS and 100 U/ml penicillin and 100 μg/ml streptomycin.

Human HepG2 liver cells (ATCC, LGC Standards GmbH), human embryonic kidney (HEK293T) cells (ATCC, LGC Standards GmbH) and *human HeLa cells* (ATCC, LGC Standards GmbH) were cultured in DMEM (# 31,966, Gibco, Life Technologies) supplemented with 10% FBS and 100 U/ml penicillin and 100 μg/ml streptomycin. Cells were seeded into 12-well plates (# 3513, Corning, Fisher Scientific, Schwerte, Germany) and treated with RSV or vehicle control.

Human adult low calcium high temperature keratinocyte cells (HaCaT) and *ARE clone 7 HaCaT* cells were kindly provided by Unilever (Sharnbrook, U.K.). ARE clone 7 HaCaT cells were revived in DMEM (# 31966, Gibco, Life Technologies) supplemented with 10% FBS. The next day, culture medium was changed to selective medium (DMEM with 10% FBS and 400 μg/ml Hygromicin B (# 10687-010, Life Technologies)) for continued growth. HaCaT cells were cultured in DMEM (# 21068-028, Life Technologies) supplemented with 1% FBS, 2 mM L-glutamine (Biochrom), 1 mM sodium pyruvate (# 11360-039, Life Technologies), 70 μM calcium chloride (Merck GmbH, Darmstadt, Germany), 100 U/ml penicillin and 100 μg/ml streptomycin.

All cell lines were maintained at 37 °C in a humidified 5% CO_2 atmosphere and treated at 60% confluence. The following passages were used: NHEK cells p 1, NHDF cells p 2–5, ARE clone 7 HaCaT cells p 7, HaCaT cells p 47, HT-29 cells p 27, HepG2 cells p 9, and HEK293T cells p 23. Hela cells at various passages were kindly provided by Dr. David Meierhofer.

2.3. Analysis of integrity of RSV

The Fluor-de-Lys SIRT1 Fluorometric Drug Discovery Assay (BML-AK555–0001, Enzo Life Sciences, Lörrach, Germany) was used to analyse the integrity of RSV after incubation in diverse solvents according to manufacturer's instructions. Briefly, compounds were added to a mixture of NAD^+ and Fluor-de-Lys (FdL) peptide in reaction buffer (RB). Reaction was started by addition of SIRT1 in RB followed by 30 min incubation at 37 °C. Reaction was stopped by addition of NAM and DeveloperII solution. After additional incubation for 45 min at 37 °C, fluorescence was measured (360/460 nm) using the POLARstar Omega (BMG LABTECH, Ortenberg, Germany).

2.4. Time-dependent decay of RSV (cell-free)

The time-dependent decay of RSV in diverse solvents was analysed using the POLARstar Omega (BMG LABTECH) at 37 °C. Samples were transferred (100 μl/well) into a UV-Star 96-well plate (# 655801, Greiner Bio-one, Frickenhausen, Germany) for kinetic and spectral measurement (between 220 and 720 nm, $\Delta\lambda$ 2 nm). Photos of RSV under various conditions (Fig. S1a and b) to document initial decay overnight were taken after about 17.5 h.

2.5. Measurement of ROS (cell-free)

The CellROX Green dye (C10444, Life Technologies) was used to quantify the formation of extracellular ROS. The dye exhibits a high fluorescence response in particular to hydroxyl radicals (HO•). Upon oxidation by ROS and after binding to nucleic acids the probe exhibits green photostable fluorescence. The CellROX Green dye is compatible with cell culture medium and requires no cellular processing, hence it can be used for measurement of ROS

generation in a cell-free environment. The dye was diluted to 10 μM/well in presence of 1 μg/ml lambda DNA (Life Technologies) prior to addition of the indicated compounds. Measurement was performed in a final volume of 150 μl/well in black 96-well plates (# 655090, Greiner Bio-One). The dye was protected against atmospheric oxygen by adding a sealing layer of 100 μl/well mineral oil (Luxcel Biosciences). Fluorescence intensity (Ex 485/30; Em 530/10) was recorded at 37 °C for 16 h using the POLARstar Omega (BMG LABTECH). For data analyses in GraphPad Prism 5.0 fluorescence signals were background-subtracted and normalized to vehicle control. Finally, signals were plotted in GraphPad Prism 5.0 either using a second order neighbour smoothing (4 neighbours) for kinetic depiction or the area under the curve (AUC) was calculated for summed depiction.

2.6. Quantification of intracellular ROS

Formation of intracellular ROS was quantified using dye 5-(and-6)-chloromethyl-2′,7′-dichlorodihydrofluorescein diacetate (CM-H_2DCFDA, Life Technologies) according to the manufacturer's instructions. In detail, NHEK cells were seeded in a 96-well plate (TPP, Biochrom) with a density of 10,000 cells/well. The following day, adherent cells were washed once with pre-warmed PBS and loaded with 50 μM dye diluted in PBS. For successful incorporation and activation of CM-H_2DCFDA, cells were incubated for 30 min at 37 °C. Afterwards, free dye was removed by washing with pre-warmed PBS. KGM (100 μl/well) was added and cells were once more incubated for 60 min at 37 °C. Compounds were added as indicated and fluorescence (Ex 485/30; Em 530/10) was measured for 16 h of treatment at 37 °C using the POLARstar Omega (BMG LABTECH).

For quantification of intracellular ROS in pre-conditioned NHEKs, cells were seeded in a 96-well plate (TPP, Biochrom) with a density of 10,000 cells/well and were pre-treated with 50 μM RSV or vehicle for 16 h. The following day, adherent cells were washed once with pre-warmed PBS and loaded with 50 μM dye diluted in PBS. For successful incorporation and activation of CM-H_2DCFDA, cells were incubated for 30 min at 37 °C. Afterwards, free dye was removed by washing with pre-warmed PBS. KGM (100 μl/well) was added and cells were once more incubated for 60 min at 37 °C. Putative protection of NHEKs against oxidative stress by RSV pre-treatment was tested by adding ethanol (0.781% v/v) or potent thiol-scavenger HNE [18] at indicated concentrations. Fluorescence (Ex 485/30; Em 530/10) was measured for 21 h of treatment using the POLARstar Omega (BMG LABTECH) at 37 °C. For data analyses in GraphPad Prism 5.0 fluorescence signals were background-subtracted and normalized to vehicle control. Finally, signals were plotted in GraphPad Prism 5.0 using a second order neighbour smoothing (4 neighbours) for kinetic depiction, or the area under the curve (AUC) was calculated for summed depiction.

2.7. Analysis of H_2O_2 generation (cell-free)

To determine generation of hydrogen peroxide (H_2O_2) the Amplex Red Glucose/Glucose Oxidase Assay Kit (A22189, Life Technologies) and the Hydrogen Peroxide Assay Kit (K265-200, BioVision, BioCat, Heidelberg, Germany) were applied. DMEM samples were filtered using Amicon Ultra-0.5 Centrifugal Filter Unit with Ultracel-10 membrane (UFC501024) or MultiScreen Ultracel-10 Filter Plate 10 kD (MAUF01010, both Merck Chemicals). For each experiment a H_2O_2 standard curve was generated. Samples were mixed with provided dye, horseradish peroxidase (HRP) and RB. Fluorescence was measured after 10–30 min incubation at RT using the POLARstar Omega (BMG LABTECH).

2.8. Analysis of superoxide generation (cell-free)

The MitoSOX Red Mitochondrial Superoxide Indicator (M36008, Life Technologies) was used to quantify the formation of superoxide ($O_2^{\bullet-}$). The dye is readily and specifically oxidized by superoxide and exhibits red photostable fluorescence after binding to nucleic acids. The probe is compatible with cell culture medium and in combination with lamda DNA (Life Technologies) applicable for measurement of superoxide generation in a cell-free environment. The dye was diluted to 10 μM/well in presence of 200 ng/well lambda DNA (Life Technologies) prior to addition of indicated compounds. Measurement was performed in a final volume of 150 μl/well in black 96-well plates (# 655090, Greiner Bio-One). The dye was protected against atmospheric oxygen by adding a sealing layer of 100 μl/well mineral oil (Luxcel Biosciences). Fluorescence intensity (Ex 485/30; Em 530/10) was recorded for 16 h at 37 °C using the POLARstar Omega (BMG LABTECH). For data analyses in GraphPad Prism 5.0 fluorescence signals were background-subtracted and normalized to vehicle control. Finally, signals were plotted in GraphPad Prism 5.0 using a second order neighbour smoothing (4 neighbours).

2.9. Viability assay

For determination of cellular viability NHEK cells were seeded in a black 96-well plate (# 353219, BD Biosciences, Heidelberg, Germany) with a density of 10,000 cells/well and a final volume of 200 μl/well. NHDF, HepG2 and THP-1 cells were seeded in a black 384-well plate (# 3712, Corning, Fisher Scientific) with a density of 2500 cells/well (NHDF) and 5000 cells/well (HepG2, THP-1), respectively, and a final volume of 25 μl/well. The following day, medium was renewed and cells were treated with the indicated compounds in a final volume of 100 μl/well (NHEK) and 35 μl/well (NHDF, HepG2, THP-1), respectively. After 16 h of treatment, cell viability was quantified using the CellTiter-Fluor Cell Viability Assay (G6081, Promega, Mannheim, Germany). Fluorescence intensity was measured (410/520 nm) using the POLARstar Omega (BMG LABTECH). Data were fitted (dashed line) using GraphPad Prism 5.0 with variable Hill slope according to equation:

$$Y = Bottom + \frac{(Top - Bottom)}{\left(1 + 10^{((logIC_{50}-X)*Hill\ Slope)}\right)}$$

Fluorescence intensity values were transformed to the relative number of cells. IC_{50} is the concentration required for a 50% inhibition of viability.

2.10. RNA isolation, reverse transcription and quantitative real-time PCR

RNeasy Mini Kit (QIAGEN, Hilden, Germany) was applied to isolate total RNA according to the manufacturer's instructions. For cell lysis 10 μl/ml β-mercaptoethanol was added to RLT buffer. Genomic DNA was digested on a column using DNase-Set (QIAGEN). The concentration of extracted RNA was measured using the Nanodrop ND-2000 Spectrophotometer (Thermo Fisher Scientific). RNA was reversely transcribed into cDNA applying the High Capacity cDNA Reverse Transcription Kit (Life Technologies) with random primers. After an initial denaturation at 95 °C for 10 min, the cDNA was amplified by 40 cycles of PCR (95 °C, 15 s; 60 °C, 60 s). Quantitative PCR was carried out with the ABI Prism 7900HT Sequence Detection System using the Power SYBR Green PCR Master Mix (all Life Technologies). The relative gene expression levels were normalized using β-actin gene and quantified by the $2^{-\Delta\Delta Ct}$ method [19]. Primer sequences are summarized in Table S5. Data were analysed using GraphPad Prism 5.0.

2.11. Knockdown of NRF2 or SIRT1 with small interfering RNA

NHEK cells were seeded into 6-well plates (Corning) and transfected with 30 nM Silencer Pre-designed siRNA Nrf2 (# 16708), Silencer Pre-designed siRNA SIRT1 (# 136457) or Silencer Select negative control siRNA (# 4390844, all Ambion, Life Technologies) using Lipofectamin 2000 transfection reagent (# 11668019, Life Technologies). Transfection was carried out in 1 ml for 48 h in KGM, whereby 0.5 ml KGM were added after 24 h. Medium was then renewed and cells were treated with 50 μM RSV or vehicle for 16 h prior to RNA and protein collection. Data were analysed using GraphPad Prism 5.0.

2.12. Genome-wide gene expression analyses

Genome-wide gene expression analyses were executed by ATLAS Biolabs GmbH (Berlin, Germany) using HumanHT-12 Expression BeadChips (Illumina, Eindhoven, The Netherlands). All basic expression data analyses were carried out applying GenomeStudio V2011.1 (Illumina). Raw data were background-subtracted and normalized using the cubic spline algorithm. Processed data were filtered for significant detection (P value ≤ 0.01) and differential expression vs. vehicle treatment according to the Illumina t-test error model, and were corrected according to the Benjamini-Hochberg procedure (P value ≤ 0.05) with the GenomeStudio software. Gene expression data were submitted to the Gene Expression Omnibus database (GSE72119).

Gene Set Enrichment Analysis (GSEA) [20] of the RSV gene expression profiles was performed using the following parameters: 1000 gene set permutations, weighted enrichment statistic, and signal-to-noise metric. Microarray data were analysed using the curated C2 KEGG pathways gene sets (version 4.0, 186 gene sets) from the Molecular Signature Database (MSigDB) (Table S2).

2.13. Cell cycle analyses

Analyses of cell cycle regulation were performed in NHEK cells treated with the indicated compounds for 16 h. Trypsinised cells were fixed in 70% ethanol (v/v) and incubated on ice for 15 min. Fixed cells were then resuspended in propidium iodide (PI)/RNase staining solution (# 4087, Cell Signalling Technology, New England Biolabs, Frankfurt, Germany), incubated for 15 min at RT and stored at $-20\,°C$ until use. Finally, cells were measured in the Accuri C6 flow cytometer (BD Biosciences). Data analyses were performed using the Watson pragmatic model in FlowJo 7.6 (Tree Star).

2.14. Phosphatidylserine externalization (Annexin V) assay

To quantify apoptosis, the externalization of phosphatidylserine [21] was determined in NHEK cells treated with the indicated compounds for 16 h by staining with annexin-V-FLUOS and propidium iodide using the Annexin-V-FLUOS Staining Kit (Roche Diagnostics, Mannheim, Germany) and subsequent flow cytometry (Accuri C6, BD Biosciences). Analyses were performed using FlowJo 7.6 (Tree Star).

2.15. Immunoblotting

NHEKs were lysed in 50 mM Tris-HCl (pH 8.0), 10 mM EDTA, 1% SDS with protease inhibitors (Roche Diagnostics) and phosphatase inhibitors (Sigma Aldrich), and sonicated (using a device from Bandelin electronic, Berlin, Germany). After centrifugation for 10 min at 10,000g, supernatants were stored at $-80\,°C$ until use. Samples were denatured and separated using a NuPAGE Novex 4–12% Bis-Tris gel (Life Technologies) and blotted onto Hybond ECL nitrocellulose membranes (GE Healthcare, Freiburg, Germany). Membranes were blocked for 1 h at RT according to the manufacturer's protocol and washed in TBS-T (0.1% w/v). Primary antibodies against P-Nrf2 (ab76026, Abcam, Cambridge, UK), Nrf2 (sc-13032X, Santa Cruz, Heidelberg, Germany), Sirt1 (MAb-063-050, Diagenode, Seraing, Belgium), P-Sirt1 (# 2314), CDK 4 (# 2906), cyclin D1 (# 2926), CDK 2 (# 2546), cyclin E2 (# 4132), p21 (# 2947), cyclin A2 (# 4656), caspase 7 (# 9492), cleaved caspase 7 (# 8438), caspase 9 (# 9502), cleaved caspase 9 (# 7237), PARP (# 9542), cleaved PARP (# 5625, all from Cell Signalling Technology) and b-Actin (sc-47778, Santa Cruz) were diluted in TBS-T (0.1% w/v) with milk powder and BSA, respectively, according to the manufacturer's protocol. Membranes were shaken at $4\,°C$ overnight, washed 3 times with TBS-T (0.1% w/v) and subsequently incubated with anti-rabbit IgG-HRP (sc-2004, Santa Cruz) and anti-mouse IgG-HRP (sc-2005, Santa Cruz), respectively, according to the manufacturer's protocol. Detection was carried out with Western Lightning ECL solution (Perkin Elmer, Rodgau, Germany). Membranes were stripped with Restore Plus Western Blot Stripping Buffer (Thermo Scientific, Life Technologies) for 5–7 min. Densitometric analysis was performed with FUSION-SL Advance 4.2 MP System (Peqlab, Erlangen, Germany).

2.16. Detection of lipid peroxidation

Click-iT Lipid Peroxidation Imaging Kit-Alexa Fluor 488 (C10446, Life Technologies) was used to determine the development of cellular lipid peroxides. Linoleamide alkyne (LAA, alkyne-modified linoleic acid) is incorporated into cellular membranes and oxidized upon lipid peroxidation, eventually resulting in proteins labelled with an azide-modified Alexa Fluor 488 dye. Increasing fluorescence intensities correspond to enhanced lipid peroxidation upon treatment. NHEK cells were seeded in 25 cm^2 cell culture flasks (Corning) and treated with 50 μM RSV or vehicle for 16 h in presence of 50 μM LAA. After trypsinisation, cells were washed with PBS and fixed in 3.7% formaldehyde (v/v) for 15 min at RT. Cells were washed in PBS, permeabilised by use of 0.5% (v/v) Triton X-100 in PBS for 10 min and subsequently blocked by adding 1% BSA (w/v) for 30 min (all at RT). Remaining BSA was removed by rigorously washing the cells with PBS. Pelleted cells were then incubated with 500 μl Click-iT reaction cocktail for 30 min at RT according to the manufacturer's protocol. The Click reaction was stopped by adding 1% (w/v) BSA/PBS. The cells were washed and resuspended with PBS. Flow cytometry was performed on the Accuri C6 (BD Biosciences). Data were analysed using FlowJo 7.6 (Tree Star) and GraphPad Prism 5.0.

2.17. Antioxidant assay

The Antioxidant Assay (# 709001, Cayman Chemical) was conducted according to the manufacturer's manual. The assay was miniaturized to a final volume of 60 μl/well. Samples including 6-hydroxy-2,5,7,8-tetramethylchroman-2-carboxylic acid (Trolox) standards were mixed with metmyoglobin and chromogen. The reaction was initiated by adding hydrogen peroxide and incubated 5 min at RT on a shaker. Finally, the absorbance was detected at 405 nm with the POLARstar Omega (BMG LABTECH). Trolox standard curve was used to convert RSV results into Trolox equivalents and data were fitted (dashed line) using linear regression model. Data were analysed using GraphPad Prism 5.0.

2.18. Quenching of RSV effects

NHEK cells were seeded in 150 cm^2 cell culture flasks (Corning) and treated with 50 μM RSV, vehicle alone or in combination with

indicated concentrations of GSH, respectively, for 16 h. Trypsinised cells were subjected to quantitative real-time PCR and measured in the Accuri C6 flow cytometer (BD Biosciences). Data were analysed using GraphPad Prism 5.0 and FlowJo 7.6 (Tree Star).

2.19. Intracellular glucose quantification

Intracellular concentration of glucose was determined using the PicoProbe Glucose Fluorometric Assay Kit (K688-100, Biovision, BioCat). NHEK cells were seeded into 25 cm² cell culture flasks (Corning, Fisher Scientific) and treated with 50 μM RSV or vehicle for 16 h. Samples were processed according to the manufacturer's instructions and deproteinised using the Deproteinising Sample Preparation Kit (K808-200, Biovision, BioCat). The assay was miniaturized to 10% of the initial volume and conducted in a clear, small-volume 384-well plate (# 784101, Greiner Bio-one). Fluorescence (535/585 nm) was measured after 45 min at 37°C using the POLARstar Omega (BMG LABTECH). Samples were normalized to protein content. Data were fitted (dashed line) using linear regression model in GraphPad Prism 5.0.

2.20. Intracellular pyruvate quantification

Intracellular pyruvate concentration was determined using the Pyruvate Assay Kit (# 700470, Cayman Chemical). NHEK cells were seeded in 150 cm² cell culture flasks (Corning) and treated with 50 μM RSV or vehicle for 16 h. Sample preparation was done according to the manufacturer's instructions. Fluorescence (530/585 nm) was measured after 20 min using the POLARstar Omega (BMG LABTECH) at 37 °C. Samples were normalized to protein content. Data were analysed using GraphPad Prism 5.0.

2.21. Intracellular lactate quantification

Lactate content was quantified with the Lactate Assay Kit (# 700510, Cayman Chemical). NHEK cells were seeded in 150 cm² cell culture flasks (Corning) and treated with 50 μM RSV or vehicle for 16 h. Sample preparation was done according to the manufacturer's instructions. Fluorescence (530/585 nm) was measured using the POLARstar Omega (BMG LABTECH) at 37 °C. Samples were normalized to protein content. Data were analysed using GraphPad Prism 5.0.

2.22. Analyses of intracellular ADP and ATP

The ADP Colorimetric/Fluorometric Assay Kit (K355-100) and ATP Colorimetric/Fluorometric Assay Kit (K354-100, both Biovision, BioCat) were used to quantify intracellular ADP and ATP content. Briefly, NHEK cells were seeded into 150 cm² cell culture flasks (Corning) and treated with 50 μM RSV or vehicle for 16 h. Flasks were washed once with ice cold PBS prior to harvest using a dispenser (TPP, Biochrom). Cell suspensions were centrifuged at 1000g for 5 min at 4 °C and resuspended in ice-cold extraction buffer, aliquoted and stored at −20 °C until usage. The assay was miniaturized to 10% of the initial volume and conducted in a clear, small-volume 384-well plate (# 784101, Greiner Bio-one) according to the manufacturer's protocol. Optical density was measured after 45 min at 37°C at 570 nm using the POLARstar Omega (BMG LABTECH). Samples were normalized to protein content. Data were analysed using GraphPad Prism 5.0.

2.23. Intracellular NAD⁺ and NADH quantification

Intracellular NAD⁺ and NADH content was analysed using the colorimetric NAD/NADH Quantitation Kit (Biovision, BioCat) according to the manufacturer's instructions. Briefly, NHEK cells

were seeded into 150 cm² cell culture flasks (Corning) and treated with 50 μM RSV or vehicle for 16 h. Flasks were washed once with ice cold PBS prior to harvest using a dispenser (TPP, Biochrom). Cell suspensions were centrifuged at 1000g for 5 min at 4 °C and resuspended in ice-cold extraction buffer. Afterwards, cells were lysed by two freeze-thaw-cycles, followed by intensive vortexing and centrifugation at 20,800g for 15 min at 4 °C. Part of the cell lysate was incubated at 60 °C for 30 min to generate NAD⁺. Cycling buffer, enzyme mix and developer were added according to the manufacturer's protocol. Optical density was measured after 30 min at 660 nm using the POLARstar Omega (BMG LABTECH). Samples at RT were normalized to protein content. Data were analysed using GraphPad Prism 5.0.

2.24. Analyses of intracellular NADP⁺ and NADPH

The NADP/NADPH-Glo Assay Kit (G9081, Promega) was used to quantify the intracellular NADP⁺ and NADPH content. NHEK cells were seeded into 12-well plates and treated with 50 μM RSV or vehicle for 16 h. The following day, cells were washed once in PBS, 60 μl PBS/well were added and cells were lysed in 60 μl base solution with 1% (w/v) dodecyl(trimethyl)azanium bromide (DTAB, D8638, Sigma Aldrich). Afterwards, 50 μl lysate were transferred into a clear 96-well plate to measure NADP⁺ and NADPH individually according to the manufacturer's protocol. Finally, 30 μl sample were transferred to a white-walled clear-bottom 384-well plate (# 781098, Greiner Bio-one) and 30 μl of NADP/NADPH-Glo Detection Reagent were added. Luminescence was measured after 30 min at RT using the POLARstar Omega (BMG LABTECH). Samples were normalized to protein content. Data were analysed using GraphPad Prism 5.0.

2.25. Analyses of intracellular reduced and oxidized glutathione

Intracellular reduced (GSH) and oxidized (GSSG) glutathione were quantified using the GSH/GSSG-Glo Assay Kit (V6611, Promega). NHEK cells were seeded in a 96-well plate (TPP) with a density of 30,000 cells/well. The following day, cells were treated with 50 μM RSV or vehicle for 16 h. The assay was miniaturized to 25% of the initial volume and conducted according to the manufacturer's protocol. In brief, cell culture medium was removed, 12.5 μl/well Total Glutathione Lysis Reagent or Oxidized Glutathione Lysis Reagent were added and incubated for 5 min at RT while shaking. Afterwards, 12.5 μl/well Luciferin Generation Reagent were added and incubated at RT for 30 min. Samples and standards were transferred to a white 96-well plate (# 655083, Greiner Bio-one) and 25 μl Luciferin Detection Reagent were added. Luminescence was measured after 15 min at RT using the POLARstar Omega (BMG LABTECH). Samples were normalized to protein content. Data were analysed using GraphPad Prism 5.0.

2.26. Oxygen consumption assay

Analyses of oxygen consumption was conducted by using the cell impermeable, oxygen-sensing fluorophore MitoXpress Xtra (Luxcel Biosciences). NHEK cells were seeded in 96-well plates (TPP, Biochrom) with a density of 25,000 cells/well. The day after, cells were treated with 50 μM RSV or vehicle for 16 h and afterwards equilibrated for 20 min under CO_2-free conditions at 37 °C. After aspirating cell culture medium, 62.5 nM/well MitoXpress Xtra diluted in KGM (LONZA) was added. The plate was incubated for 10 min under CO_2-free conditions at 37 °C. Compounds were added as indicated and each well was sealed with 100 μl HS Mineral Oil (Luxcel Biosciences). Dual-read time-resolved fluorescence (TR-F) was measured (380/650 nm) with the POLARstar Omega (BMG LABTECH) at 37 °C. Lifetime, dual-delay and gate

times were calculated and set according to the manufacturer's instructions. Data were analysed using GraphPad Prism 5.0.

2.27. Fluorescence microscopy

NHEK cells were seeded in X-well tissue culture chambers (Sarstedt, Nürnbrecht, Germany) at a density of 20,000 cells/well. One day later, adherent cells were treated for 16 h with the indicated compounds. Visualization of MAP1LC3A, Actin, Nrf2, Keap1, GCLC and GSR was executed as recently described in Weidner et al. [22]. In brief, cells were washed with PBS (Sigma Aldrich) and fixed in 4% (v/v) formaldehyde/PBS (Sigma Aldrich) for 15 min at RT. Cells were washed with PBS (Sigma Aldrich), permeabilised in 0.3% (v/v) Triton X-100/PBS (PBS-Tx) for 10 min at RT, washed with PBS and afterwards blocked in 5% (v/v) goat serum (Sigma Aldrich) in PBS-Tx for 60 min at RT. Afterwards, cells were incubated with primary antibodies at 4 °C overnight. Primary antibodies and dilutions were as follows: MAP1LC3A (1:100; AP1801d-ev-AB, Biovision, BioCat), Nrf2 (1:100; sc-13032X, Santa Cruz; 1:100), Keap1 (1:100, sc-365626, Santa Cruz), GCLC (1:100, ab41463, Abcam) and GSR (1:100, sc-133159, Santa Cruz). Subsequently, cells were washed with PBS-Tx and stained with anti-mouse IgG (H+L) F(ab')2 fragment Alexa Fluor 555 Conjugate (# 4409, Cell Signalling Technology) and anti-rabbit IgG (H+L), F(ab') 2 fragment Alexa Fluor 488 Conjugate (# 4412, Cell Signalling Technology) diluted (1:1000) in 1% (w/v) BSA/PBS-Tx for 1h at RT in the dark. Cells were washed with PBS for 5 min, and the MAP1LC3A stained cells were counterstained with F-actin probe Texas Red-X Phalloidin (1:100, T7471, Life Technologies) for 20 min at RT in the dark. Cells were washed with PBS, the chamber was removed from the slide, samples were counterstained with Pro-Long Gold Antifade Mountant (with DAPI) solution (Life technologies), a cover slip applied (# 235503704, Duran Group, Wertheim/Main, Germany) and incubated at RT for 24 h. Fluorescence microscope imaging was performed using the LSM700 microscope (Zeiss, Jena, Germany).

2.28. Redox potential, redox state and redox environment

To calculate the half-cell reduction potential of a selected redox couple the Nernst equation (Eq. (1)) was used and transformed to match the experimental conditions (T = 310K = 37 °C, pH 7) (Eq. (2)).

$$\Delta E = \Delta E^0 - \frac{RT}{nF} * lnQ \tag{1}$$

$$E_{hc} = E^{0'} - \frac{61.5 \text{ mV}}{n} * logQ \tag{2}$$

R is the gas constant ($8.314 \text{ J K}^{-1} \text{ mol}^{-1}$), T the temperature in Kelvin, n the number of electrons exchanged, F the Faraday constant ($9.6485 * 10^4 \text{ C mol}^{-1}$), and Q the mass action expression. As the standard reduction potential (E^0, $E^{0'}$) is pH dependent, an adjustment is necessary:

$$E_{pH} = E^{0'} + \left[(pH - 7.0) * \frac{\Delta E}{\Delta pH} \right] \tag{3}$$

E_{pH} represents the half-cell reduction potential at a given pH, while $\Delta E / \Delta pH$ is dependent on the number of electrons and protons involved. The half-cell reduction potential of a selected redox couple can eventually be determined according to (Eq. (5)).

$$E_{hc} = E_{pH} - \frac{61.5 \text{ mV}}{n} * log \frac{[reduced \; species]}{[oxidized \; species]} \tag{4}$$

$$E_{hc,pH} = E^{0'} + \left[(pH - 7.0) * \frac{\Delta E}{\Delta pH} \right] - \frac{61.5 \text{ mV}}{n}$$
$$* log \frac{[reduced \; species]}{[oxidized \; species]} \tag{5}$$

The half-cell reduction potential can be calculated for the following metabolites (redox couples):

$$Pyruvate + 2H^+ + 2e^- \longrightarrow Lactate \quad E^{0'} = -190 \text{ mV}$$
$$E_{hc,pH} = -190 \text{ mV} + [(pH - 7.0) * -61.5 \text{ mV}] - \frac{61.5 \text{ mV}}{2} * log \frac{[lactate]}{[pyruvate]} \tag{6}$$

$$NAD^+ + H^+ + 2e^- \longrightarrow NADH \quad E^{0'} = -320 \text{ mV}$$
$$E_{hc,pH} = -320 \text{ mV} + \left[(pH - 7.0) * -30.75 \text{ mV} \right] - \frac{61.5 \text{ mV}}{2} * log \frac{[NADH]}{[NAD^+]} \tag{7}$$

$$NADP^+ + H^+ + 2e^- \longrightarrow NADPH \quad E^{0'} = -320 \text{ mV}$$
$$E_{hc,pH} = -320 \text{ mV} + \left[(pH - 7.0) * -30.75 \text{ mV} \right] - \frac{61.5 \text{ mV}}{2} * log \frac{[NADPH]}{[NADP^+]} \tag{8}$$

$$GSSG + 2H^+ + 2e^- \longrightarrow 2GSH \quad E^{0'} = -240 \text{ mV}$$
$$E_{hc,pH} = -240 \text{ mV} + [(pH - 7.0) * -61.5 \text{ mV}] - \frac{61.5 \text{ mV}}{2} * log \frac{[GSH]^2}{[GSSG]} \tag{9}$$

Finally the redox environment was calculated using the redox couple 2GSH/GSSG alone (Fig. 5a and Table S4) or redox couples lactate/pyruvate, NADH/NAD$^+$ and 2GSH/GSSG (Fig. S7d and Table S4), respectively.

To relate the reduced redox environment to an oxidative challenge, we conducted a thought experiment focusing on oxidation of ethanol to acetaldehyde and simultaneous ROS generation [23–25]:

$$Acetaldehyde + 2H^+ + 2e^- \longrightarrow Ethanol \quad E^{0'} = -195 \text{ mV}$$
$$E_{hc} = -195 \text{ mV} - \frac{61.5 \text{ mV}}{2} * log \frac{[Ethanol]}{[Acetaldehyde]}$$
$$E_{ethanol} = -195 \text{ mV} - 30.75 \text{ mV} * log \frac{[Ethanol]}{[Acetaldehyde]} \tag{10}$$

In order to estimate the amount of ROS induced by application of ethanol, which can be minimized by RSV pre-treatment, we made the following assumptions:

- pH 7,
- T = 37 °C,
- 2GSH/GSSG redox couple is the driving force of the redox environment and
- Consider concentrations of GSH and GSSG as measured at pH 7.0026 (vehicle) and 7.0632 (RSV), respectively.

At equilibrium, change of the half-cell reduction potentials of both couples equal 0 and can be transformed appropriately:

$$\Delta E_{GSH} = \Delta E_{Ethanol} = 0 \tag{11}$$

$$\Delta E_{GSH} = -195 \text{ mV} - 30.75 \text{ mV} * logQ_{RSV} - \left(-195 \text{ mV} - 30.75 \text{ mV} * logQ_{Vehicle} \right)$$
$$\Delta E_{GSH} = -195 \text{ mV} - 30.75 \text{ mV} * logQ_{RSV} + 195 \text{ mV} + 30.75 \text{ mV} * logQ_{Vehicle}$$
$$\Delta E_{GSH} = -30.75 \text{ mV} * logQ_{RSV} + 30.75 \text{ mV} * logQ_{Vehicle} \tag{12}$$

According to Sarkola et al. (2002) [26] the formation of acetaldehyde in humans is dependent on the amount of ethanol. The mean slope can be determined as follows:

$$0.13 \frac{\mu M \; Acetaldehyde}{mM \; Ethanol} = \frac{0.13 \mu M \; Acetaldehyde}{1000 \; \mu M \; Ethanol} \tag{13}$$

We can use this information to calculate $Q_{Vehicle}$:

$$Q_{Vehicle} = \frac{[Ethanol]}{[Acetaldehyde]} = 7692.\,3$$

$$\longrightarrow \qquad logQ_{Vehicle} = 3.\,886$$

$$\longrightarrow 30.\,75\ mV * logQ_{Vehicle} = 119.5 \qquad (14)$$

Finally we can calculate Q_{RSV} accordingly:

$$E_{GSH_{RSV}} - E_{GSH_{Vehicle}} = -30.\,75\ mV * logQ_{RSV} + 119.\,5 \qquad (15)$$

$$E_{GSH_{RSV}} - E_{GSH_{Vehicle}} - 119.\,5 = -30.\,75\ mV * logQ_{RSV}$$

$$Q_{RSV} = 10^{\frac{E_{GSH_{RSV}} - E_{GSH_{Vehicle}} - 119.5}{-30.75mV}}$$

$$Q_{RSV} = 9745.\,9 \qquad (16)$$

$$Q_{Vehicle} = 7,\,692.\,3 = 100\%$$

$$Q_{RSV} = 9,\,745.\,9 = 126.\,7\% \quad \| + 26\% ethanol \qquad (17)$$

Thus, we can estimate that owing to RSV pre-treatment and the resulting shift in redox environment, NHEKs are likely to tolerate roughly 26% more ethanol than vehicle-treated cells. Notably, in particular vehicle-treated NHEK cells did not tolerate higher doses of ethanol without serious reduction of viability. Consequently, experimental evidence for this thought experiment cannot be provided completely.

We further challenged RSV pre-treated NHEKs with HNE, a potent thiol scavenger [18,27,28]. Assuming that one molecule GSH is needed to detoxify one molecule HNE, we can roughly estimate the amount of additional HNE quenched owing to increased cellular concentrations of GSH after RSV pre-treatment. Corresponding to the increasing GSH content (7 μmol per g protein, roughly 2 μM) due to pre-treatment with RSV, the observed pre-conditioning effect is depleted at HNE concentrations $\geq 25\ \mu M$. Nevertheless, this is just an approximation, as the GSH pool regulates the reduction state of many biological molecules and because HNE can efficiently react with many intracellular thiol groups, lipids and proteins present in the biological system.

2.29. Statistical analyses

Data are expressed as mean ± standard error (s.e.m.), if not otherwise denoted. Statistical tests were performed in GraphPad Prism 5.0. For comparison of two groups statistical significance was examined by unpaired two-tailed Student's t-test. One-way ANOVA with subsequent Dunnett's post-test was used for multiple comparisons. A P value ≤ 0.05 was defined as statistically significant.

3. Results and discussion

3.1. RSV is unstable under physiologically relevant conditions

The vast majority of studies seem to assume specific RSV-target protein interactions, which implies that RSV remains intact during treatments. However, after incubation in various media containing physiological concentrations of sodium bicarbonate (NaHCO₃), a key component of water as well as buffer of blood and biological cells, RSV reacts efficiently, as indicated by striking yellowish colour changes (Fig. S1a and b). Light absorbance at characteristic RSV maximum (308 nm) decreased rapidly in water and cell culture media, both containing sodium bicarbonate (Fig. S1c and d, Table S1). After 16 h incubation the absorption maximum of RSV was almost completely diminished. Furthermore, using a

commonly applied fluorescence-based SIRT1 assay no enzymatic activation could be detected (Fig. S1e).

Oxidation of RSV at atmospheric oxygen level (21% O_2, as usually applied in cell culture) [16,29] could potentially be considered as non-physiological as in blood vessels the oxygen amount is roughly 14% and in tissues or tumours even lower ($\sim 1\%$ O_2) [30]. Our data suggest that the auto-oxidation of RSV is highly dependent on the presence of sodium bicarbonate and pH of the solvent [14,31] (see Figs. 1 and 2 in Reference [31]), whereas a decreased oxygen partial pressure seems to have a comparably minor influence (see Figs. 3 and 4 in reference [31]). These data suggest that oxidation of RSV can to some extent even take place in hypoxic microenvironments.

These results corroborate widely ignored findings that the stability and oxidation of RSV in physiologically relevant media is strongly influenced by pH and in particular the availability of hydroxyl anions [16,29,32]. Interestingly, RSV reacted also efficiently in tap water (Figs. S1e and S2e left), which might in part explain the often-reported perplexing low bioavailability of RSV in vivo [33–35]. Although RSV could potentially be protected from protein carriers such as serum albumin [36], the entirety of these data makes it difficult to understand how RSV could exert compound-protein specific effects. These results further indicate that metabolisation of RSV, for example by oxidation of the enzymes of the CYP1 family, might play a minor role in physiological context, consistent with the usually extremely low amounts of detected metabolites of RSV [33–35].

3.2. RSV produces ROS under physiologically relevant conditions

We next asked how the oxidizing RSV could induce relevant biological effects. Notably, treatment of cells with RSV resulted in time- and concentration-dependent generation of intracellular ROS (Fig. 1a and b, Fig. S2a).

Owing to the complexity of biological matrices it remains technically impossible to detect exactly the entirety of unstable intermediate ROS. However, using defined solvents or a cell-free environment, we detected significantly increased amounts of ROS, including superoxide ($O_2^{\bullet-}$), hydroxyl radicals (HO$^\bullet$) and hydrogen peroxide (Fig. 1c, Fig. S2b-e) [14,16]. For example, between 5.0 and 12.5 μM hydrogen peroxide (Fig. S2e) was generated depending on the concentration of RSV and sodium bicarbonate (Fig. S2e left), whereas (metabolic) scavengers such as pyruvate strongly depleted ROS (Fig. S2e right). As revealed by an anti-oxidant assay using trolox as control compound, in presence of sodium bicarbonate the anti-oxidative feature of RSV was clearly diminished (Fig. S2f left). In contrast, RSV showed roughly 2-fold higher anti-oxidative capacity in solvents lacking sodium bicarbonate (Fig. S2f right). These data suggest that RSV loses in part its anti-oxidative properties and becomes more pro-oxidative in physiological media. Notably, low concentrations of oxidation products of RSV can mildly affect cellular biomolecules such as proteins and lipids (Fig. 1d).

In summary, these data indicate that oxidation of RSV takes place under physiologically relevant conditions. These conditions differ significantly from many experimental setups that are applied to analyse RSV by common bicarbonate-free enzymatic assays, and also vary from bicarbonate-free crystallization procedures that are in general used for x-ray analyses.

3.3. Effects on primary human keratinocytes

We next asked how oxidation of RSV might exert biological effects. Given the here observed oxidative features in particular topological application of RSV seems a medically relevant approach, as is also evident from the number of available
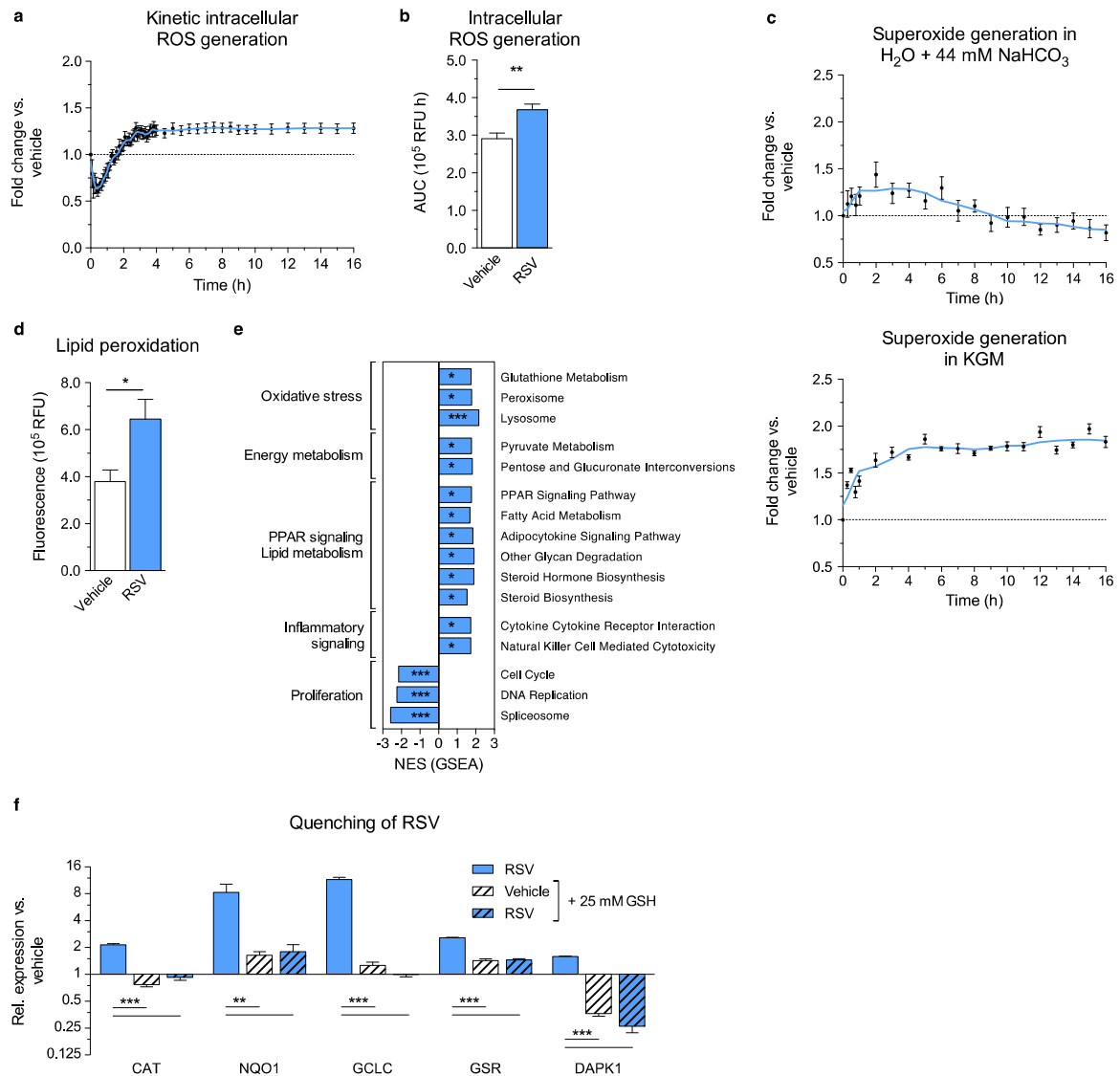
Fig. 1. RSV produces ROS and triggers cellular defense. (a and b) Kinetic (a) and summed (b) intracellular generation of ROS in primary NHEK cells after administration of 50 μM RSV. Values are mean ± s.e.m. (n=6); AUC, area under the curve; RFU, relative fluorescence units. (c) Generation of superoxide in H_2O and keratinocyte growth medium (KGM), which both contain sodium bicarbonate ($NaHCO_3$), after addition of 50 μM RSV for indicated time periods. Values are mean ± s.e.m. (n=4). (d) RSV (50 μM) induced lipid peroxidation in NHEKs. Values are mean ± s.e.m. (n=4); *$P < 0.05$ versus vehicle. (e) Selection of enriched KEGG pathways in NHEKs treated with 50 μM RSV using gene set enrichment analysis (GSEA). Values are normalized enrichment scores (NES, n=4 for vehicle, n=3 for RSV); *$P < 0.05$, **$P < 0.01$, ***$P \leq 0.001$ versus vehicle. See also Table S2. (f) GSH considerably quenched effects of RSV on gene expression. Values are mean ± s.e.m. (n=4); **$P < 0.01$; ***$P \leq 0.001$ one-way ANOVA versus RSV.

dermatological products based on RSV. We thus focused in this study on potential protection of the human epidermis. Notably, due to ethical considerations and law, for physiological testing dermatological research applies *ex vivo* models such as the here applied primary human keratinocytes that formed the outer layer of the skin of a patient. Keratinocytes are known to build a tight layer of cells that can be used as epidermal grafts (Fig. S2g) [37], and these cells represent a prime target for lotions and emollients based on RSV [38,39].

Firstly, we investigated potential oxidation of cellular components owing to oxidation products of RSV. Sixteen hours of treatment with 50 μM RSV slightly elevated lipid peroxidation in normal human primary keratinocyte (NHEK) cells, indicating mildly increased oxidation of cellular biomolecules (Fig. 1d).

Moreover, to globally monitor cellular response to oxidation products of RSV, genome-wide RNA expression analyses revealed a slight but significantly increased expression of molecular pathways covering oxidative stress response and inflammatory signalling, as well as fatty acid metabolism (Fig. 1e and Table S2). In

contrast, processes linked to proliferation, DNA replication and cell cycle were down-regulated. Importantly, quenching of oxidation by adding strong reducing molecules such as 25 mM synthetic GSH significantly reversed expression of cell response marker genes (Fig. 1f). As shown in a control experiment, quenching by synthetic GSH reduced the levels of ROS derived from RSV in a cell-free environment (Fig. S2h) and within cells (Fig. S2i), suggesting that these ROS caused the observed gene expression events. As tested with a small panel of unrelated cell models, despite cell-specific defense mechanisms the here observed gene expression responses seem to some degree be independent from cellular background (Fig. S3a–d, Table S3).

These data indicate to our knowledge for the first time that major gene expression events induced by RSV can be explicitly attributed to the development of oxidation products, since application of molecular quenchers suppressed these effects. The oxidative effects of RSV analysed here in mammalian cells might also underlie phytoalexin-based protection of plants against microbial infection [40].

3.4. Oxidative products of RSV cause hormetic effects

In a next step, we asked how oxidation products derived from RSV could potentially influence viability of cells. Using cell viability assays, we observed increased cellular fitness up to about 50 μM RSV in treated NHEKs, whereas higher concentrations tended to produce toxic effects, leading to a typical bi-phasic, hormetic dose-viability curve (Fig. 2a and b). Notably, in additional cellular models for fibroblasts and liver cells we observed similar bi-phasic dose-viability curves with varying susceptibility to RSV treatment (Fig. 2c–d). Slight but significantly increased expression of molecular markers for oxidative stress response, such as catalase (CAT), could be observed up to 100 μM RSV with a maximum at 50 μM RSV (Fig. 2b). On the other hand, too high concentrations of RSV (> 100 μM RSV) resulted in low cell viability (Fig. 2b). In summary, these data are in line with a large body of mostly unconsciously reported hormetic cellular effects of RSV [10].

Importantly, the hormetic dose-viability curve was significantly truncated by adding 25 mM synthetic GSH as a quencher, providing to our knowledge for the first time strong evidence that increased cellular viability mainly derives from ROS and other oxidation products of RSV (Fig. 2a–d).

Further concentration- and time-dependent treatments of NHEKs resulted in generally slight up-regulation of a number of metabolic, aging, oxidative stress and inflammation signalling genes (Figs. 3a–d and S3e–h). Notably, in NHEKs these cellular responses could be observed in a concentration range of approximately 5–100 μM RSV. Strong changes in gene expression were observed after at least 12 h, most obviously after 16 h of treatment.

The entirety of the data suggests that under physiological conditions increased viability of cells was triggered by ROS (and potentially also other radicals of RSV). Instead of the conventional pharmacological (linear) threshold model we observed a bi-phasic

mode of action of RSV: at normally applied non-toxic concentrations, RSV treatment increased cellular fitness owing to expression of cellular defense genes, whereas higher concentrations of RSV resulted in toxic effects. The underlying reason for this cellular behaviour seems to depend largely on the pro-oxidative properties of RSV. In summary, the here proposed link introduces an explicit explanation of the so far rather "nebulous" hormetic effects of RSV.

3.5. Hormetic effects of oxidative products derived from RSV are driven by activation of Nrf2

We next asked how oxidising RSV could induce specific cellular response. Especially the nuclear factor (erythroid-derived 2) like 2 (Nrf2) is considered responsible for accommodating oxidative stress (Fig. S4a) [2,41–43]. Consistent with the above shown production of oxidation products of RSV, we observed translocation of redox-sensitive Nrf2 into the nucleus of NHEKs (Figs. 3e and S4b), leading to regulation of known Nrf2 target genes (Fig. 3a–d bold font). Remarkably, knockdown of mRNA expression of Nrf2 gene by small interfering RNAs (siRNAs) significantly decreased the observed effects of RSV on gene expression response (Figs. 3f and S5a). This experiment indicates that Nrf2 via its well-established canonical signalling pathway mediates major response of NHEKs to the oxidation products of RSV.

ROS and further radicals can produce numerous effects by increasing oxidation of cellular biomolecules, leading for example to inhibition of protein activity. Thus, we expected multiple defense mechanisms to counteract ROS including for example autophagy and cell cycle arrest. Interestingly, RSV treatment slightly increased autophagy, probably to degrade and recycle potentially damaged cellular components (Figs. 4a and S5b), corroborating previous observations [44]. Simultaneously, primary NHEKs were partly arrested in G1 cycle phase (Figs. 4b and S5c). Interestingly,
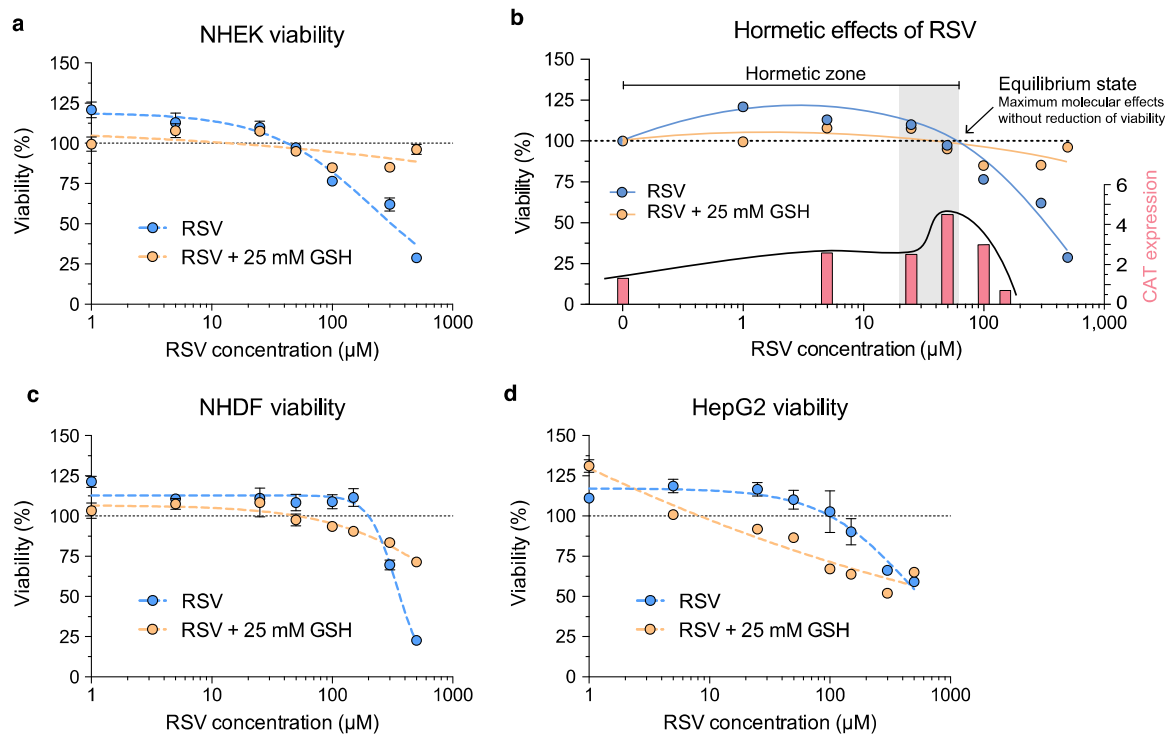
Fig. 2. Hormetic effects are induced by generation of ROS derived from RSV. (a) After 16 h of treatment RSV increased viability at low concentrations but decreased viability of NHEKs at concentrations ≥ 50 μM (IC$_{50}$: 223.8 μM). RSV effects on viability were considerably quenched by GSH (IC$_{50}$: 247,747.0 μM). Values are mean $\pm$ s.e.m. (n=3). (b) Dose-response curve of RSV in treated NHEKs (blue). Hormetic zone emerges from 1 to 60 μM RSV and highest molecular effects (gene expression peaks of oxidative stress response gene catalase (CAT)) were generally observed at 50 μM RSV. (c) RSV started decreasing the viability of NHDF cells at concentrations ≥ 300 μM (IC$_{50}$: 342.5 μM), which was quenched by GSH (IC$_{50}$: 1163.0 μM). Values are mean $\pm$ s.e.m. (n=6). (d) RSV started reducing the viability of human HepG2 liver cells at concentrations ≥ 150 μM (IC$_{50}$: 445.3 μM), whereas GSH quenched the RSV induced effects. Values are mean $\pm$ s.e.m. (n=6).

the cells did not show any signs of senescence or apoptosis (Figs. 4c and d, S5d and e) and exhibited reduced necrosis (Fig. 4d).

In the context of slightly increasing molecular stress, the here observed mechanisms might allow cells to focus their limited resources on cellular repair, while decreasing cellular proliferation and nucleotide synthesis (Fig. 1e). Notably, similar effects were reported for mild stress such as calorie restriction to improve cellular fitness [45,46].

We next asked if and how other reported factors such as the promiscuously reacting lysine deacetylase sirtuin 1 (SIRT1) could potentially modulate the effects derived from RSV-based activation of Nrf2, for example in the context of autophagy.

As shown above, under physiologically relevant conditions the almost completely degraded RSV can merely directly or allosterically induce the enzymatic activity of SIRT1 (Fig. S1e). However,

the 4-fold up-regulation of SIRT1 expression (Fig. 3b), the phosphorylated SIRT1 (Fig. S6a) and the simultaneously increased $NAD^+/NADH$ ratio (Figs. 5a and S7d) might concurrently contribute to modify the mild effects derived from oxidized RSV. Knockdown of the SIRT1 gene resulted in 20% lower expression of NRF2, suggesting a potential modifying effect of SIRT1 on Nrf2 (Fig. S6b). However, at least in NHEKs knockdown of SIRT1 did not strongly influence overall gene or protein expression (Fig. S6c and d), corroborating the major role of Nrf2 in the response to oxidative products of RSV.

3.6. Oxidative products of RSV induce a reduced cellular redox environment

We then asked how gene expression induced by RSV/ROS-
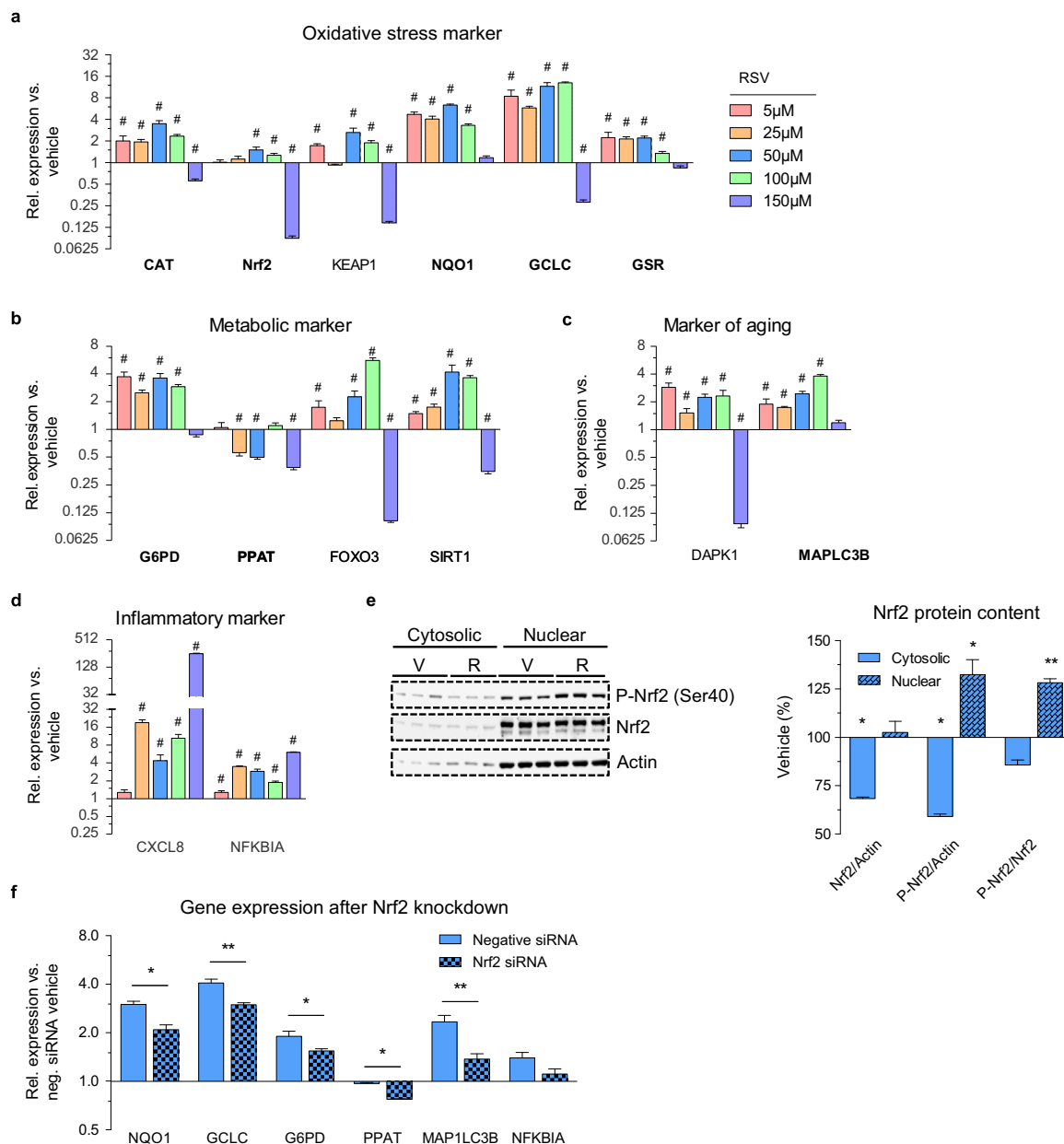
Fig. 3. Cellular response to RSV-derived oxidation products including ROS is mediated by the redox-sensitive transcription factor Nrf2. (a, b, c and d) Concentration-dependent effects of RSV in NHEK cells after 16 h. Values are mean ± s.e.m. (n=4); # $P < 0.05$ versus vehicle. Nrf2 and its target genes are marked in bold font. See also Fig. S3. (e) Translocation of Nrf2 and increased amount of nuclear phosphorylated Nrf2 as well as nuclear Nrf2 protein. Densitometric analysis of immunoblots relative to vehicle, with all gels run under the same experimental conditions and cropped blots are depicted. Values are mean ± s.e.m. (n = 4), ** $P < 0.01$. V, vehicle; R, RSV. (f) Quantification of gene expression after knockdown of Nrf2 in RSV treated (16 h) NHEKs. Values are mean ± s.e.m. (n=4); * $P < 0.05$, ** $P < 0.01$, *** $P ≤ 0.001$ one-way ANOVA versus negative siRNA vehicle. See also Fig. S5a.

triggered activation of Nrf2 might influence cellular metabolism. In NHEKs treated for 16 h with 50 μM RSV, we observed signalling events such as increased phosphorylation of pyruvate dehydrogenase E1 component subunit alpha (PDE1α) at serine 293 (Fig. S7a), an effect known to inhibit endogenous pyruvate breakdown and oxidative phosphorylation [47]. Consequently, this molecular effect led to increased intracellular levels of the potential ROS-scavenger pyruvate while lactate remained at constant levels (Fig. 5a). We further observed under constant mitochondrial biogenesis decreased mitochondrial oxygen consumption during 16 h of RSV treatment (Fig. S7b and c).

Moreover, the intracellular ratio of metabolite couples GSH/GSSG and ATP/ADP, as well as the amount of glucose and pyruvate, were significantly increased (see Figs. 5a and S7d). Moreover, the intracellular ratios of metabolite couples NADH/NAD$^+$ and NADPH/NADP$^+$ were significantly decreased (Fig. S7d). Consistent with the ratio of the most relevant GSH/GSSG redox couple, the expression of genes and proteins related to glutathione metabolism was highly elevated, corresponding to significantly raised levels of the potent cellular antioxidant GSH (Figs. 5a and b, S7d and e).

In summary, these data indicate a metabolic switch that leads in particular to an increased pool of reduced glutathione (GSH). Clearly, the GSH concentration can vary a lot between different cell types, depending for example on stress exposure and function [48].

To explore thermodynamic aspects of the cellular state, we next analysed the redox environment of NHEKs treated with RSV. Therefore, we considered intracellular concentrations of above-mentioned key metabolites, using the Eq. (18) [48].

$$Redox\ environment = \sum_{i=1}^{n(couple)} E_i * [reduced\ species]_i \tag{18}$$

Indeed, via activation of the canonical Nrf2 pathway RSV treatment at hormetic concentrations increased in particular the level of endogenously produced GSH. This effect resulted in a shift of the cellular redox environment to a more reduced state (Fig. 5c and for calculation-relevant parameters see Table S4) [49]. Based on the GSH/GSSG couple, which provides the most relevant cellular pool of reducing equivalents [48], we calculated a slight shift of redox environment of −2.61 mV mmol GSH per gram protein. A similar trend was observed by taking into account further redox couples (see also Fig. S7f and Table S4). According to our results, RSV treatment can eventually contribute to an overall chemical reduction of biological molecules containing for example thiol groups, as evident from the increased cellular GSH concentration (Fig. 5a).
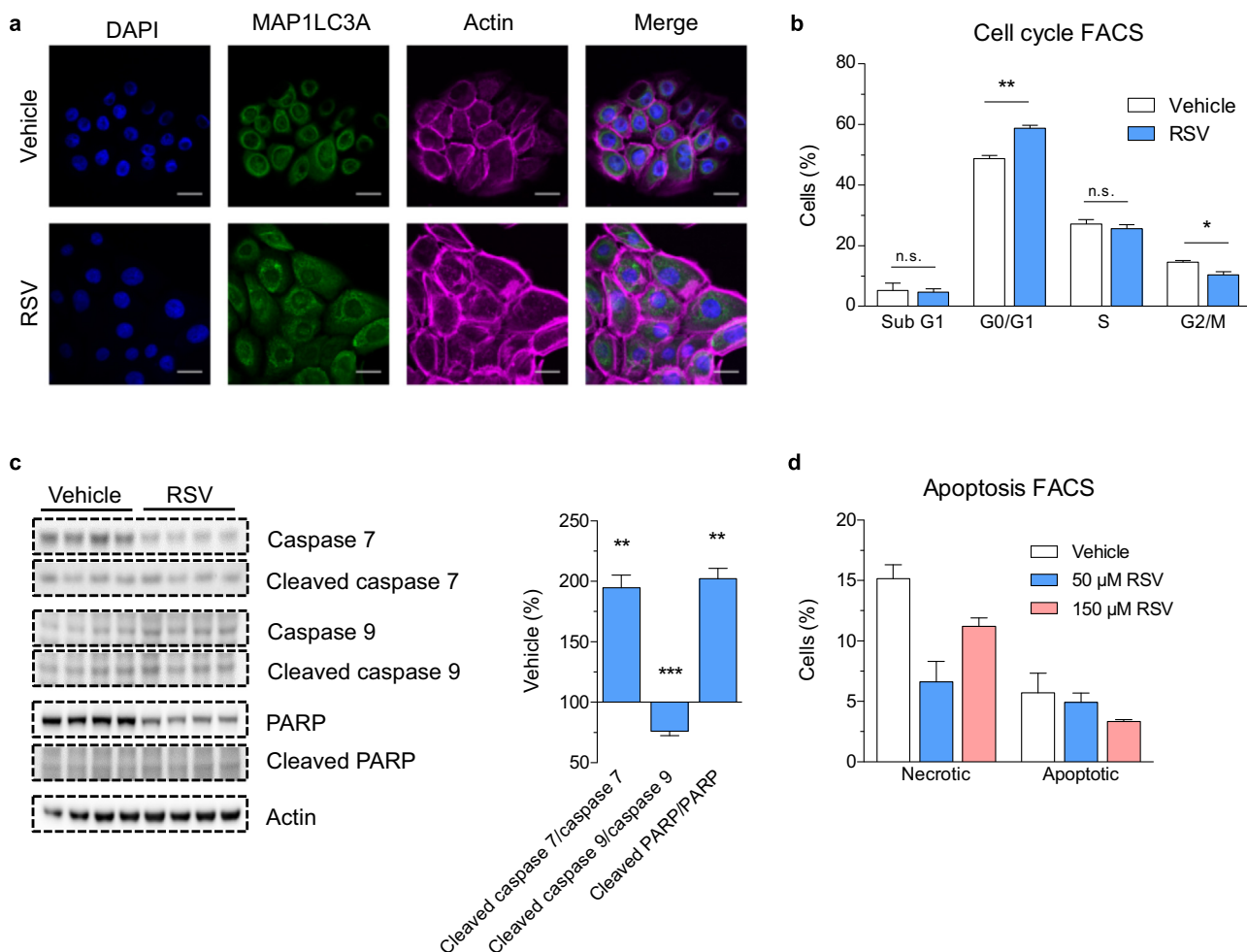
Fig. 4. RSV induced autophagy and G1 phase cell cycle arrest but did not cause apoptosis in NHEK cells. (a) Fluorescence staining marking DAPI (blue), microtubule-associated protein 1 light chain 3A (MAP1LC3A, green) and Actin (magenta) in RSV treated NHEKs. See also Fig. S5b. (b) G1 phase cell cycle arrest in NHEKs after 16 h of treatment with 50 μM RSV. Values are mean ± s.e.m. (n=4); *P < 0.05; **P < 0.01, ***P ≤ 0.001 versus vehicle. See also Fig. S5c. (c) RSV substantially increased the ratio of caspase 7 and PARP suggesting slight apoptosis. All gels were run under the same experimental conditions and cropped blots are depicted. Values are mean ± s.e.m. (n=4); *P < 0.05, **P < 0.01, ***P ≤ 0.001 versus vehicle. (d) None of the tested RSV concentrations did induce apoptosis after 16 h of treatment of NHEKs, but 150 μM RSV tended to increase the proportion of necrotic cells. Values are mean ± s.e.m. (n=2). See also Fig. S5e.
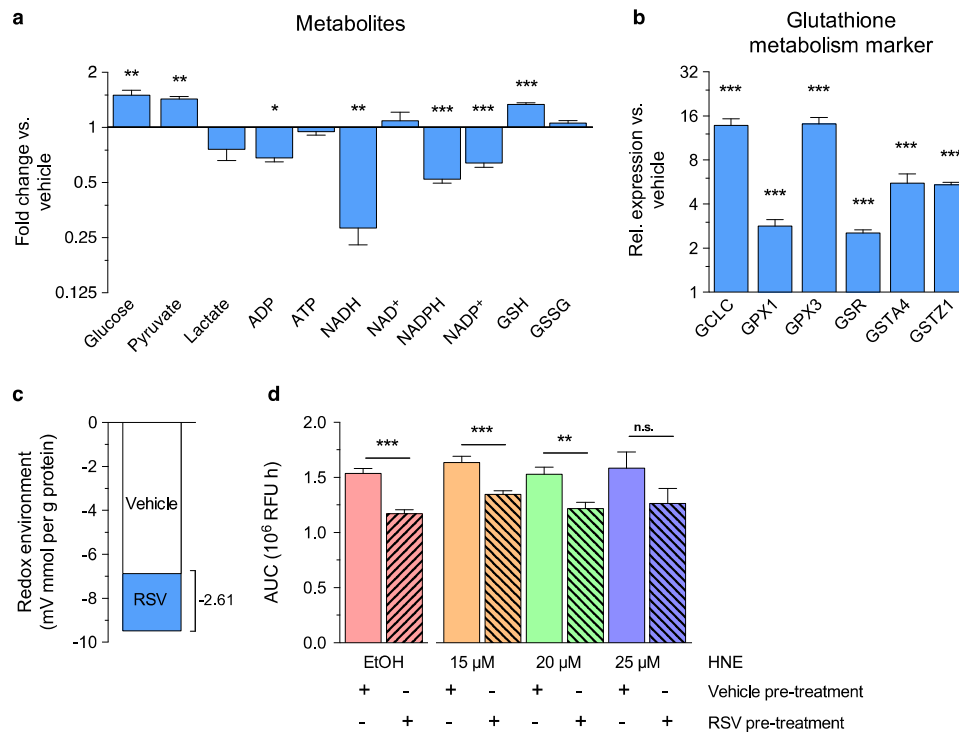
Fig. 5. RSV influenced the concentration of key metabolites to shift the cellular redox environment to a reduced state, thereby increasing robustness versus oxidative stress. (a) Shift in intracellular metabolite concentrations after treatment with 50 μM RSV for 16 h in NHEKs. Values are mean ± s.e.m. (NADH, NAD$^+$ n=3; glucose, ATP, ADP, GSH, GSSG n=4; lactate, pyruvate, NADPH, NADP$^+$ n=5); *$P < 0.05$, **$P < 0.01$; ***$P \leq 0.001$ versus vehicle. See also Fig. S7d. (b) RSV substantially induced gene expression of glutathione metabolism marker genes, thereby increasing the intracellular GSH pool. Values are mean ± s.e.m. (n=4); ***$P \leq 0.001$ versus vehicle. (c) GSH/GSSG ratio was used to calculate the redox environment. See also Table S4 and for calculation with various metabolites Fig. S7f. (d) Pre-treatment of NHEKs with 50 μM RSV for 16 h decreased intracellular generation of ROS after subsequent treatment with ethanol (0.78%), while increasing concentrations of thiol/GSH-scavenger HNE revised the cellular capacity to counteract oxidative stress. Values are mean ± s.e.m. (n=7); **$P < 0.01$, ***$P \leq 0.001$ versus vehicle. AUC, area under the curve; RFU, relative fluorescence units.

In summary, the often-observed pleiotropic effects of RSV can be subsumed by the redox environment equation (Eq. (18)) to explain and quantify a major (thermodynamic) state of the cellular system. In the ideal case the redox environment of the cell can be calculated by making use of the full "redoxome" and not only selected metabolite data, which might become possible in the future. Furthermore, exact knowledge of the concentrations of the various (reductive) metabolites such as GSH could be used to generate kinetic molecular networks of the cell.

We finally analysed if the observed reduced redox environment could potentially protect the cell from (oxidative) stress. Therefore, we subjected NHEKs to 16 h pre-treatment with 50 μM RSV. After replacement of medium the NHEK cells were devoid of any residual RSV. We then treated NHEKs with 0.78% ethanol and analysed the endogenous generation of intracellular ROS from cellular metabolisation of ethanol, i.e. the level of oxidative stress (Fig. 5d) [24]. Notably, we observed that overall reduced cellular environment (owing to the increased pool of endogenous GSH) enabled RSV-pre-treated NHEKs to buffer additional production of ROS resulting from biotransformation of ethanol (Fig. 5d). The protective effects of pre-treatment with RSV, i.e. the raise of endogenously produced GSH, were revised in a concentration-dependent manner by addition of 4-hydroxy-2-nonenal (HNE). This α,β-unsaturated aldehyde mainly acts as a strong electrophile by depleting cellular sulfhydryl compounds like GSH (Fig. 5d), and might also interact with Nrf2 [28,50,51].

4. Conclusion

Summarizing, we propose a bi-phasic pharmacological model for RSV, which might also be relevant for other pro-oxidative

polyphenols. This model comprises i) generation of oxidation products at non-toxic concentrations in physiologically relevant, sodium bicarbonate-containing media, ii) specific mediation of cellular response to pro-oxidative RSV by the redox-sensitive transcription factor Nrf2 and iii) induction of gene expression programs resulting in slight reductive shifting of cellular redox-environment to protect the cell from additional (oxidative) stress (Fig. 6a and b).

Clearly, the here described model largely depends on the pro- and anti-oxidative properties of RSV in a given microenvironment. We argue that bicarbonate containing media are essential for living systems (from simple micro- to higher mammalian organisms), and thus it seems that the pro-oxidative features of RSV might be relevant for a large variety of biological phenomena. Given that the here shown chemical properties of RSV appear dominant, we assume that not only mammalian but also microbial enzymatic conversion of RSV might be probably less important than previously anticipated. Our data indicate that analysis of the pro- and anti-oxidative features of RSV shall be thoroughly explored prior any biological investigation and interpretation.

And what about applications? In particular the human epidermis being predominantly prone to external stress might benefit from dermatological application of RSV. The here elaborated pro-oxidative features of RSV and the redox-environment shifting concept can at least in part explain such recent claims [43]. Of note, whereas RSV might remain stable under low pH conditions in the stomach (see Figs. 1 and 2 in Reference [31]), physiologically well-known neutralization in the duodenum – by high concentrations of bicarbonate derived from the pancreas – might induce efficient oxidation of RSV in the intestine.

Considering the increase of endogenously produced GSH and resulting reduction of the cellular redox environment as the main
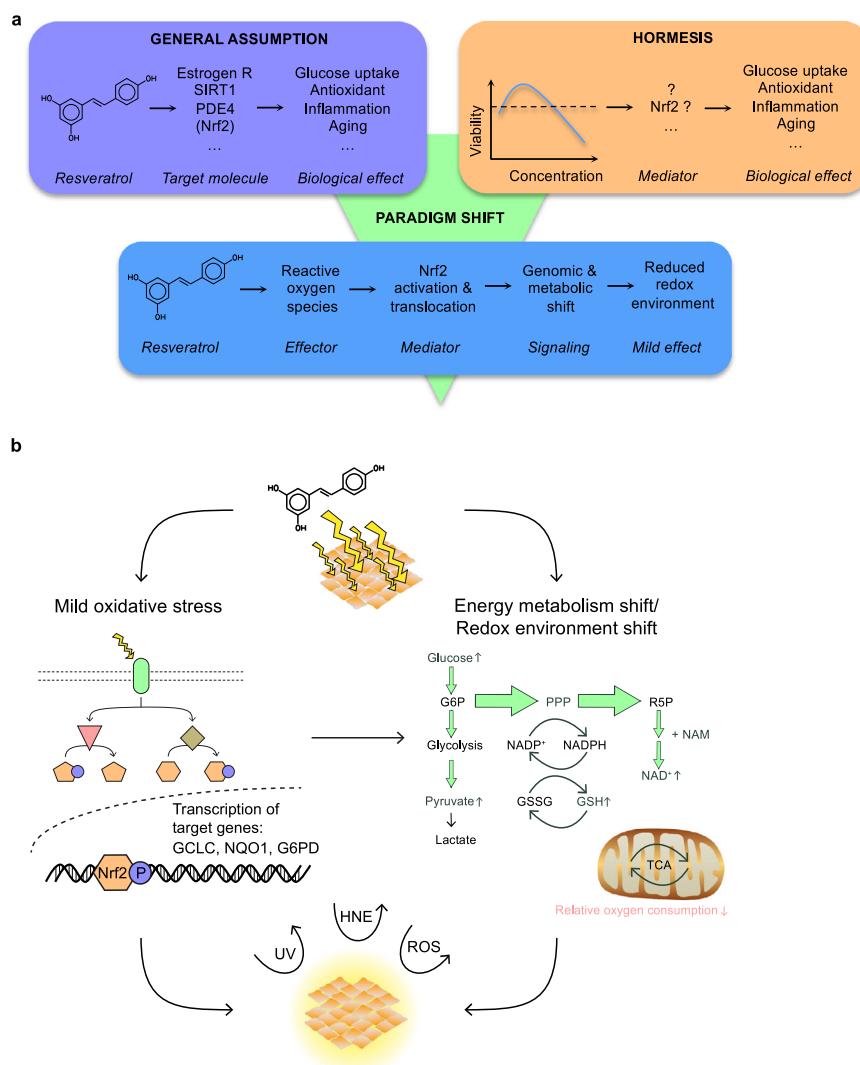
Fig. 6. Model and molecular networks involved in RSV-induced cytoprotection against oxidative stress. (a) A dose–dependent compound-target protein model is generally assumed to explain biological effects of RSV. Our model instead integrates pro-oxidative features of RSV, Nrf2-mediated cellular response and mild beneficial (hormetic) biological effects at normally applied concentrations. Estrogen R=estrogen receptor, SIRT1=silent mating type information regulation 2 homolog 1, PDE4=phosphodiesterase 4. (b) At low concentrations oxidizing RSV induces mild stress, resulting in a metabolic and redox environment shift to increase the level of endogenous quenchers such as GSH to eventually protect the cell from environmental stress.

phenomena, the often-reported weak and pleiotropic effects of RSV on biological cells can be described quantitatively and in a comprehensive manner. On the other hand, in particular the effects derived from oxidation products with short lifetimes such as ROS are difficult to trace *in vitro* and in particular *in vivo*. This drawback might provoke scepticism how such "dirty" chemicals shall exert well-controllable cellular and physiological effects.

Nevertheless, taking a (thermodynamic) systems view we suggest to apply the here explored paradigm for mathematically analysing biological effects of pro-oxidative compounds. For example, the determination of the redox environment allows for calculating the oxidation-buffering capacity of targeted cells and tissues under investigation. Using such a framework and additionally establishing kinetic networks, might be helpful approaches to rationally exploit beneficial bi-phasic effects of pro-oxidative compounds for therapeutic and preventive application. For example, this may include development of chemical derivatives of RSV and molecular carriers to efficiently guide pro-oxidative molecules to the target tissues of choice.

In general, hormetic induction of cellular fitness by pro-oxidative polyphenols such as RSV might represent a powerful approach to protect cells against physiological stress and to inhibit age-related diseases.

Accession codes

The accession number for all genome-wide gene expression data used in this study is GEO: GSE72119.

Declaration of interest

Acknowledgements

Appendix A. Supporting information

Supplementary data associated with this article can be found in the online version at http://dx.doi.org/10.1016/j.freeradbiomed.2016.08.006.

References

[1] S. Quideau, D. Deffieux, C. Douat-Casassus, L. Pouysegu, Plant polyphenols: chemical properties, biological activities, and synthesis, Angew. Chem. Int. Ed. Engl. 50 (2011) 586–621, http://dx.doi.org/10.1002/anie.201000044.

[2] M. Jang, et al., Cancer chemopreventive activity of resveratrol, a natural product derived from grapes, Science 275 (1997) 218–220, http://dx.doi.org/10.1126/science.275.5297.218.

[3] J.M. Smoliga, J.A. Baur, H.A. Hausenblas, Resveratrol and health – a comprehensive review of human clinical trials, Mol. Nutr. Food Res. 55 (2011) 1129–1141, http://dx.doi.org/10.1002/mnfr.201100143.

[4] R.A. Baxter, Anti-aging properties of resveratrol: review and report of a potent new antioxidant skin care formulation, J. Cosmet. Dermatol. 7 (2008) 2–7, http://dx.doi.org/10.1111/j.1473-2165.2008.00354.x.

[5] M. Ndiaye, C. Philippe, H. Mukhtar, N. Ahmad, The grape antioxidant resveratrol for skin disorders: promise, prospects, and challenges, Arch. Biochem. Biophys. 508 (2011) 164–170, http://dx.doi.org/10.1016/j.abb.2010.12.030.

[6] B.D. Gehm, J.M. McAndrews, P.Y. Chien, J.L. Jameson, Resveratrol, a polyphenolic compound found in grapes and wine, is an agonist for the estrogen receptor, Proc. Natl. Acad. Sci. USA 94 (1997) 14138–14143, http://dx.doi.org/10.1073/pnas.94.25.14138.

[7] K.T. Howitz, et al., Small molecule activators of sirtuins extend Saccharomyces cerevisiae lifespan, Nature 425 (2003) 191–196, http://dx.doi.org/10.1038/nature01960.

[8] S.J. Park, et al., Resveratrol ameliorates aging-related metabolic phenotypes by inhibiting cAMP phosphodiesterases, Cell 148 (2012) 421–433, http://dx.doi.org/10.1016/j.cell.2012.01.017.

[9] E.J. Calabrese, L.A. Baldwin, Hormesis: the dose-response revolution, Annu. Rev. Pharmacol. Toxicol. 43 (2003) 175–197, http://dx.doi.org/10.1146/annurev.pharmtox.43.100901.140223.

[10] E.J. Calabrese, M.P. Mattson, V. Calabrese, Resveratrol commonly displays hormesis: occurrence and biomedical significance, Hum. Exp. Toxicol. 29 (2010) 980–1015, http://dx.doi.org/10.1177/0960327110383625.

[11] D. Gems, L. Partridge, Stress-response hormesis and aging: "that which does not kill us makes us stronger", Cell Metab. 7 (2008) 200–203, http://dx.doi.org/10.1016/j.cmet.2008.01.001.

[12] E.J. Calabrese, Hormesis: from mainstream to therapy, J. Cell Commun. Signal. 8 (2014) 289–291, http://dx.doi.org/10.1007/s12079-014-0255-5.

[13] H. Erlank, A. Elmann, R. Kohen, J. Kanner, Polyphenols activate Nrf2 in astrocytes via H2O2, semiquinones, and quinones, Free Radic. Biol. Med. 51 (2011) 2319–2327, http://dx.doi.org/10.1016/j.freeradbiomed.2011.09.033.

[14] D.D. Li, et al., Hydroxyl radical reaction with trans-resveratrol: initial carbon radical adduct formation followed by rearrangement to phenoxyl radical, J. Phys. Chem. B 116 (2012) 7154–7161, http://dx.doi.org/10.1021/jp3033337.

[15] S. Stojanovic, O. Brede, Elementary reactions of the antioxidant action of trans-stilbene derivatives: resveratrol, pinosylvin and 4-hydroxystilbene, Phys. Chem. Chem. Phys. 4 (2002) 757–764, http://dx.doi.org/10.1039/b109063c.

[16] N.C. Yang, C.H. Lee, T.Y. Song, Evaluation of resveratrol oxidation in vitro and the crucial role of bicarbonate ions, Biosci. Biotechnol. Biochem. 74 (2010) 63–68, http://dx.doi.org/10.1271/bbb.90549.

[17] C.C. Winterbourn, Toxicity of iron and hydrogen peroxide: the Fenton reaction, Toxicol. Lett. 82–83 (1995) 969–974, http://dx.doi.org/10.1016/0378-4274(95)03532-X.

[18] H. Esterbauer, R.J. Schaur, H. Zollner, Chemistry and biochemistry of 4-hydroxynonenal, malonaldehyde and related aldehydes, Free Radic. Biol. Med. 11 (1991) 81–128, http://dx.doi.org/10.1016/0891-5849(91)90192-6.

[19] K.J. Livak, T.D. Schmittgen, Analysis of relative gene expression data using real-time quantitative PCR and the 2(-Delta Delta C(T)) Method, Methods 25 (2001) 402–408, http://dx.doi.org/10.1006/meth.2001.1262.

[20] A. Subramanian, et al., Gene set enrichment analysis: a knowledge-based approach for interpreting genome-wide expression profiles, Proc. Natl. Acad. Sci. USA 102 (2005) 15545–15550, http://dx.doi.org/10.1073/pnas.0506580102.

[21] V.A. Fadok, D.L. Bratton, S.C. Frasch, M.L. Warner, P.M. Henson, The role of phosphatidylserine in recognition of apoptotic cells by phagocytes, Cell Death

Differ. 5 (1998) 551–562, http://dx.doi.org/10.1038/sj.cdd.4400404.

[22] C. Weidner, et al., Melissa officinalis extract induces apoptosis and inhibits proliferation in colon cancer cells through formation of reactive oxygen species, Phytomedicine 22 (2015) 262–270, http://dx.doi.org/10.1016/j.phymed.2014.12.008.

[23] S.C. Bondy, Ethanol toxicity and oxidative stress, Toxicol. Lett. 63 (1992) 231–241, http://dx.doi.org/10.1016/0378-4274(92)90086-Y.

[24] S.M. Bailey, E.C. Pietsch, C.C. Cunningham, Ethanol stimulates the production of reactive oxygen species at mitochondrial complexes I and III, Free Radic. Biol. Med. 27 (1999) 891–900, http://dx.doi.org/10.1016/S0891-5849(99)00138-0.

[25] H.K. Seitz, F. Stickel, Molecular mechanisms of alcohol-mediated carcinogenesis, Nat. Rev. Cancer 7 (2007) 599–612, http://dx.doi.org/10.1038/nrc2191.

[26] T. Sarkola, M.R. Iles, K. Kohlenberg-Mueller, C.J. Eriksson, Ethanol, acetaldehyde, acetate, and lactate levels after alcohol intake in white men and women: effect of 4-methylpyrazole, Alcohol. Clin. Exp. Res. 26 (2002) 239–245, http://dx.doi.org/10.1111/j.1530-0277.2002.tb02530.x.

[27] S. Schreier, et al., Hydrogen sulfide scavenges the cytotoxic lipid oxidation product 4-HNE, Neurotox. Res. 17 (2010) 249–256, http://dx.doi.org/10.1007/s12640-009-9099-9.

[28] H. Esterbauer, H. Zollner, N. Scholz, Reaction of glutathione with conjugated carbonyls, Z. Nat. C 30 (1975) 466–473, http://dx.doi.org/10.1515/znc-1975-7-808.

[29] L.H. Long, M.V. Clement, B. Halliwell, Artifacts in cell culture: rapid generation of hydrogen peroxide on addition of (−)-epigallocatechin, (−)-epigallocatechin gallate, (+)-catechin, and quercetin to commonly used cell culture media, Biochem. Biophys. Res. Commun. 273 (2000) 50–53, http://dx.doi.org/10.1006/bbrc.2000.2895.

[30] M.C. Brahimi-Horn, J. Pouyssegur, Oxygen, a source of life and stress, FEBS Lett. 581 (2007) 3582–3591, http://dx.doi.org/10.1016/j.febslet.2007.06.018.

[31] A. Plauth, et al., Oxygen and pH-dependent oxidation of resveratrol, Data Brief (2016) http://dx.doi.org/10.1016/j.dib.2016.09.012, in press.

[32] S. Zupancic, Z. Lavric, J. Kristl, Stability and solubility of trans-resveratrol are strongly influenced by pH and temperature, Eur. J. Pharm. Biopharm. 93 (2015) 196–204, http://dx.doi.org/10.1016/j.ejpb.2015.04.002.

[33] O. Vang, et al., What is new for an old molecule? Systematic review and recommendations on the use of resveratrol, PLoS One 6 (2011) e19881, http://dx.doi.org/10.1371/journal.pone.0019881.

[34] E. Wenzel, V. Somoza, Metabolism and bioavailability of trans-resveratrol, Mol. Nutr. Food Res. 49 (2005) 472–481, http://dx.doi.org/10.1002/mnfr.200500010.

[35] I. Murakami, et al., Metabolism of skin-absorbed resveratrol into its glucuronized form in mouse skin, PLoS One 9 (2014) e115359, http://dx.doi.org/10.1371/journal.pone.0115359.

[36] M.S. Nair, Spectroscopic study on the interaction of resveratrol and pterostilbene with human serum albumin, J. Photochem. Photobiol. B 149 (2015) 58–67, http://dx.doi.org/10.1016/j.jphotobiol.2015.05.001.

[37] B.K. Sun, Z. Siprashvili, P.A. Khavari, Advances in skin grafting and treatment of cutaneous wounds, Science 346 (2014) 941–945, http://dx.doi.org/10.1126/science.1253836.

[38] M.J. Abla, A.K. Banga, Quantification of skin penetration of antioxidants of varying lipophilicity, Int. J. Cosmet. Sci. 35 (2013) 19–26, http://dx.doi.org/10.1111/j.1468-2494.2012.00728.x.

[39] O.V. Zillich, U. Schweiggert-Weisz, K. Hasenkopf, P. Eisner, M. Kerscher, Release and in vitro skin permeation of polyphenols from cosmetic emulsions, Int. J. Cosmet. Sci. 35 (2013) 491–501, http://dx.doi.org/10.1111/ics.12072.

[40] M.A. Kohanski, D.J. Dwyer, J.J. Collins, How antibiotics kill bacteria: from targets to networks, Nat. Rev. Microbiol. 8 (2010) 423–435, http://dx.doi.org/10.1038/nrmicro2333.

[41] H.C. Huang, T. Nguyen, C.B. Pickett, Regulation of the antioxidant response element by protein kinase C-mediated phosphorylation of NF-E2-related factor 2, Proc. Natl. Acad. Sci. USA 97 (2000) 12475–12480, http://dx.doi.org/10.1073/pnas.220418997.

[42] Z. Ungvari, et al., Resveratrol confers endothelial protection via activation of the antioxidant transcription factor Nrf2, Am. J. Physiol. Heart Circ. Physiol. 299 (2010) H18–24, http://dx.doi.org/10.1152/ajpheart.00260.2010.

[43] J. Soeur, J. Eilstein, G. Lereaux, C. Jones, L. Marrot, Skin resistance to oxidative stress induced by resveratrol: from Nrf2 activation to GSH biosynthesis, Free Radic. Biol. Med. 78 (2015) 213–223, http://dx.doi.org/10.1016/j.freeradbiomed.2014.10.510.

[44] E. Morselli, et al., Caloric restriction and resveratrol promote longevity through the Sirtuin-1-dependent induction of autophagy, Cell Death Dis. 1 (2010) e10, http://dx.doi.org/10.1038/cddis.2009.8.

[45] S. Timmers, et al., Calorie restriction-like effects of 30 days of resveratrol supplementation on energy metabolism and metabolic profile in obese humans, Cell Metab. 14 (2011) 612–622, http://dx.doi.org/10.1016/j.cmet.2011.10.002.

[46] K. Pallauf, K. Giller, P. Huebbe, G. Rimbach, Nutrition and healthy ageing: calorie restriction or polyphenol-rich "MediterrAsian" diet? Oxid. Med. Cell. Longev. 2013 (2013) 707421, http://dx.doi.org/10.1155/2013/707421.

[47] J.H. Chung, Metabolic benefits of inhibiting cAMP-PDEs with resveratrol, Adipocyte 1 (2012) 256–258, http://dx.doi.org/10.4161/adip.21158.

[48] F.Q. Schafer, G.R. Buettner, Redox environment of the cell as viewed through

the redox state of the glutathione disulfide/glutathione couple, Free Radic. Biol. Med. 30 (2001) 1191–1212, http://dx.doi.org/10.1016/S0891-5849(01)00480-4.

[49] M. Schafer, S. Werner, Nrf2-A regulator of keratinocyte redox signaling, Free Radic. Biol. Med. (2015), http://dx.doi.org/10.1016/j.freeradbiomed.2015.04.018.

[50] Y. Huang, W. Li, A.-N.T. Kong, Anti-oxidative stress regulator NF-E2-related factor 2 mediates the adaptive induction of antioxidant and detoxifying enzymes by lipid peroxidation metabolite 4-hydroxynonenal, Cell Biosci. 2 (2012) 40, http://dx.doi.org/10.1186/2045-3701-2-40.

[51] E. López-Bernardo, A. Anedda, P. Sánchez-Pérez, B. Acosta-Iborra, S. Cadenas, 4-Hydroxynonenal induces Nrf2-mediated UCP3 upregulation in mouse cardiomyocytes, Free Radic. Biol. Med. 88 (2015) 427–438, http://dx.doi.org/10.1016/j.freeradbiomed.2015.03.032.